

NOVEL VIEW VIDEO PREDICTION USING A DUAL REPRESENTATION

Sarah Shiraz, Krishna Regmi, Shruti Vyas, Yogesh S. Rawat, Mubarak Shah
Center for Research in Computer Vision (CRCV), University of Central Florida

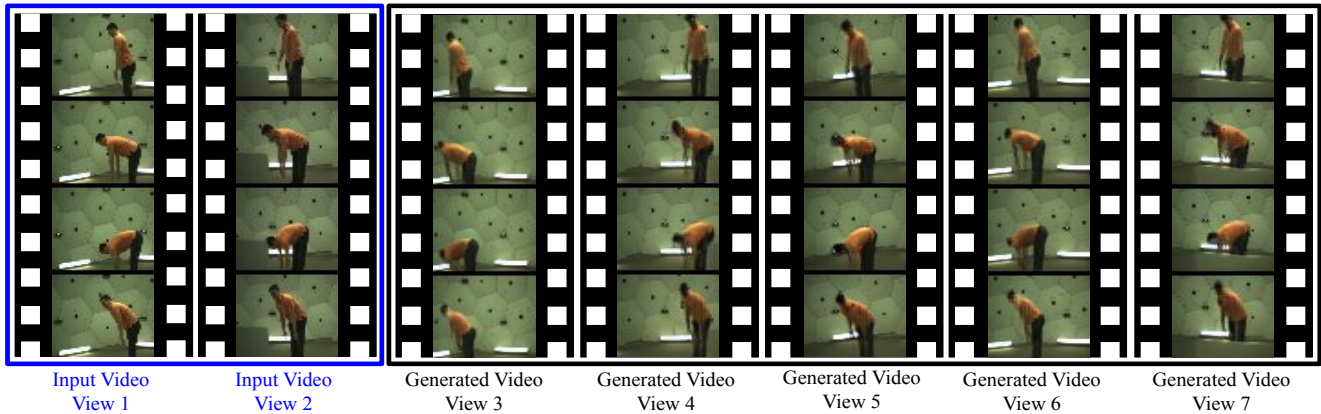


Fig. 1. Novel-view Video Prediction. Given a set of video clips from single/multiple input viewpoints, the proposed framework can generate a video clip from a novel viewpoint. In the above example, given two input views, our network is able to generate videos from multiple viewpoints, video from five unseen viewpoints are shown here.

ABSTRACT

We address the problem of novel view video prediction; given a set of input video clips from a single/multiple views, our network is able to predict the video from a novel view. The proposed approach does not require any priors and is able to predict the video from wider angular distances, upto 45 degree, as compared to the recent studies predicting small variations in viewpoint. Moreover, our method relies only on RGB frames to learn a dual representation which is used to generate the video from a novel viewpoint. The dual representation encompasses a view-dependent and a global representation which incorporates complementary details to enable novel view video prediction. We demonstrate the effectiveness of our framework on two real world datasets: NTU-RGB+D and CMU Panoptic. A comparison with the State-of-the-art novel view video prediction methods shows an improvement of 26.1% in SSIM, 13.6% in PSNR, and 60% in FVD scores without using explicit priors from target views.

Index Terms— Novel View Synthesis, Dual Representation, Video Prediction

1. INTRODUCTION

Novel view prediction finds interesting applications in robotics, graphics and augmented reality [1, 2, 3]. Given one or more input views, the task is to predict the seen observations from a novel unseen view. Ample research on novel view prediction has been done for *image based methods* [4, 5], however novel view prediction for *videos* is much more challenging and relatively unexplored. The image-based approaches, when directly applied to videos, result in temporally incoherent videos as they do not model temporal dynamics.

In this paper, we address the problem of novel view video prediction without using explicit estimation of 3D structures and geometry based transformations. Most of the video prediction works [6, 7, 8] in the literature are mainly limited to single viewpoint with the aim of improved dynamics and sharper frames. Only recently, the authors in [9] tackled the task of novel view *video* prediction by proposing the use of depth maps and human pose information of the novel view as priors. However, the availability of these priors from the query viewpoint is a big assumption which may not always be valid and requires extra computation.

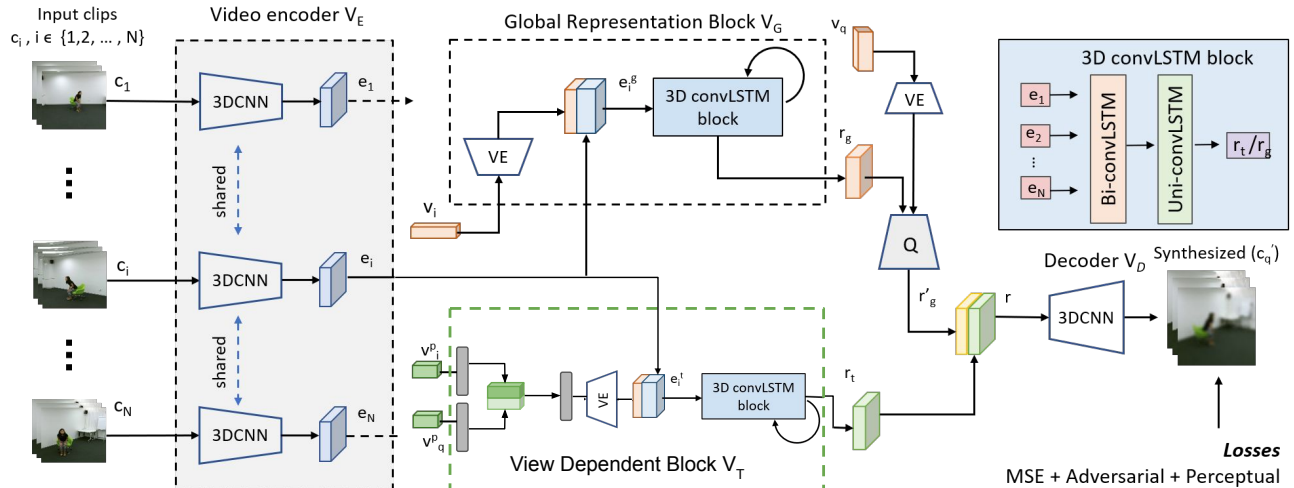


Fig. 2. Overall architecture of the proposed network. The Video Encoder V_E takes multiple input clips $c_i, i \in 1, 2, \dots, N$ from different viewpoints, v_i to learn the encoded features, e_i . The Global Representation Block, V_G uses the absolute view parameters of the input, v_i . The features e_i are aggregated with view embeddings from view embedder, VE using a 3D convLSTM block. The Query Network, Q retrieves features, r'_g according to the query view v_q . The view dependent block, V_T on the other hand uses relative view information, using both partial input view v_i^p and partial query view v_q^p , which adds fine view-dependent details to the video. The dual representation, r thus obtained by aggregating the retrieved global representation, r'_g and view dependent representation, r_t is used to synthesize the query view video, c'_q .

Considering this limitation, we propose a novel learning based method which generates human action videos from a novel view without any priors and of better video quality. Proposed method takes video clips from multiple viewpoints and utilizes a two-stream approach for learning the dual representations: global and view-dependent. The global representation focuses on the general features, such as scene structure, whereas the view-dependent representation focuses on finer details specific to the query view. We evaluate our approach with extensive ablations and report state-of-the-art results on two real world datasets, CMU Panoptic [10] and NTU-RGB+D [11]. **Contributions:** (1) We propose a novel-view video prediction framework which can generate videos from unseen query viewpoints. (2) The proposed network integrates both global as well as view-dependent representation for effective novel-view video prediction. (3) We provide extensive evaluation of our approach on two real-world datasets, CMU Panoptic [10] and NTU-RGB+D [11], achieving significant improvement over the existing methods without using any prior information about the query views. We report 26.1% improvement in SSIM, 13.6% improvement in PSNR and 60% improvement in FVD scores over state-of-the-art viewLSTM [9] on CMU-Panoptic Dataset [10].

2. RELATED WORK

Early works in multi-view prediction by Cooke *et al.* [12] and [13] create a novel view video by exploiting the scene

geometry information from multiple sources. Similar works by Domański *et al.* [14] discuss novel view video prediction from multiview video sources. [15] estimates the 3D mesh of the person present in the query view and transfer the textures from the 2D images to the mesh. Recently, Lakhal [9] guided their network to synthesize novel view videos by feeding skeleton and depth priors from the query view. Such priors are strong cues that influence the quality of synthesized videos. Learning to synthesize the novel view video without any prior information from the query view is very challenging and our work attempts to solve this problem. We do so by learning holistic as well as view-dependent representations from multiple input video clips for effective novel-view video prediction.

3. METHOD

Given a set of video clips $c_i, i \in 1, 2, \dots, N$ from a single or multiple input views, our goal is to synthesize a video clip from a novel viewpoint. We propose a deep neural network which learns a dual internal representation, r by assimilating global and view dependent information required for a novel view generation. Global information is learned in the form of a global representation r_g which encodes the scene as a whole whereas, view-dependent representation r_t helps recover the finer details specific to the query view. As shown in Figure 2, input to the proposed network is a set of N video clips from different view points along with the respective view informa-

tion, and the output is a video clip from the query view. The view information is in the form of a vector, v of dimension $N \times d$ where d is the number of view parameters for a viewpoint. The c'_q is the output clip from the query view. The network can be divided into four parts: a Video Encoder, V_E , Representation Learning Blocks V_G & V_T , and a Video Decoder V_D . Each part is explained as follow:

3.1. Video Encoder V_E

Video Encoder is a multi-view encoder that takes N video clips separately from multiple views and learns features of each video clip in parallel. We use a 3D CNN based encoder network which is a modified version of an Inflated 3D convNet [16] architecture. The encoder shares weights for all the input video clips. The input to the Encoder is c_i where $i \in [1, 2, \dots, N]$ and the output is the encoded feature e_i .

3.2. Global Representation Block V_G

The goal of this block is to transform the video features e_i in a way such that we have a global representation representing the dynamics of the overall scene. To achieve this, video encoding e_i are first concatenated with the respective view information, resulting in e_i^g , and then all features are aggregated using a recurrent network. The viewpoint, v_i , is a d -dimensional vector that contains viewpoint information *i.e.* camera location coordinates, viewpoint angle, principal point offset, focal length etc. It is passed through a View Embedder which performs linear interpolation on it before combining with the video features e_i . Next, $e_i^g, i \in [1, 2, \dots, N]$ are aggregated together using a recurrent network consisting of a bidirectional convLSTM followed by a unidirectional convLSTM to learn the global representation r_g .

3.3. View-Dependent Block V_T

The goal of the *View-Dependent Block* V_T is to transform the features of video clips from multiple input viewpoints to the features of a query viewpoint. To do so, it learns the features specific to the query view and help in adding finer details to the synthesized video. To achieve this, we use relative view information *i.e.* partial view vector v_i^p , comprising of only viewpoint angles and camera location of the input views v_i^p and the query view v_q^p . The partial viewpoint facilitates the model to focus more on the input view embeddings which are the most similar to query view. Specifically, we apply two fully-connected layers on v_i^p and v_q^p to learn the relative view features e_i^t , as shown in Figure 2. Similar to aggregation of embeddings in V_G we use a 3D convLSTM, in particular a bidirectional convLSTM followed by a unidirectional convLSTM to learn the view dependent representation r_t . However, the weights of 3D convLSTM block are not shared with V_G .

3.4. Video Decoder V_D

The goal of the Video Decoder, V_D , is to integrate the view dependent representation with the global representation to synthesize a video clip from the query view v_q . To achieve this, it uses a convolutional-based query network, Q , to extract the query view specific features r'_g from the global representation r_g and then combines it with view dependent representation r_t to get the combined representation r . Finally, we use another 3D convNet which uses r and transforms the features to the image space resulting in a synthesized video clip c'_q .

3.5. Loss Function

We use a combination of reconstruction, adversarial and perceptual loss as shown in Equation 1 to train our network.

$$\mathcal{L} = \lambda_r L_r + \lambda_p L_p + \lambda_{adv} L_{adv} \quad (1)$$

where L_r , L_p and L_{adv} are reconstruction, perceptual and adversarial losses respectively. L_p compares the features extracted from conv5_2 layer of VGG-19 [17] for ground truth and predicted video. We empirically set $\lambda_p = \lambda_{adv} = 0.01$ and $\lambda_r = 1$. To improve the realism of the synthesized video clip, we employ a discriminator which **(a)** distinguishes real video clips from the synthetically generated ones, and **(b)** it recognizes realistic motion between frames. The loss term is implemented by the minimax loss [18].

4. EXPERIMENTS

4.1. Experimental Setup

Datasets We evaluated our network on following two datasets. **(1) CMU Panoptic Dataset [10]** is a large-scale multi-activity real-world dataset with a total of 521 viewpoints. The cameras are installed in 20 hexagonal panels, with 24 cameras in each panel. The provided viewpoint information vector, v_i , consists of camera location coordinates (3D), principal point offset (2D), focal length (2D), distortion coefficients (5D), horizontal-pan (1D) and vertical-pan (1D), therefore $d = 14$. **(2) NTU-RGB+D [11]** dataset contains 60 action classes recorded from 3 viewpoints: at horizontal angles of -45 degrees, 0 degree, 45 degrees. We use the cross subject evaluation split of 40,320 and 16,560 clips for training and testing respectively. The viewpoint information vector, v_i , for this dataset, consists of camera height (1D), camera distance (1D), horizontal-pan (1D) and vertical-pan (1D), viewpoint angle (1D), therefore $d = 5$.

4.2. Novel View Video Prediction: CMU Panoptic

CMU panoptic [10] has a large number of views which makes it a lucrative dataset for cross-view video prediction. Considering this, we experiment on a large-scale setting, using

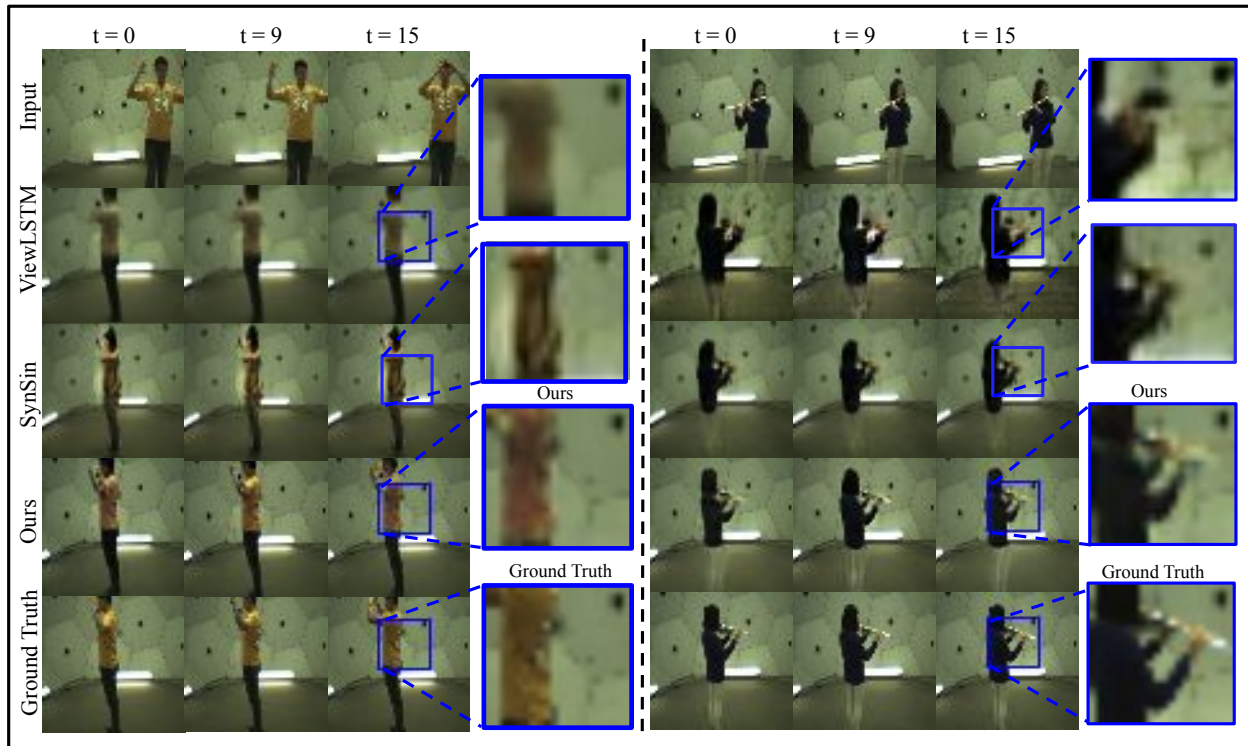


Fig. 3. Qualitative Results on CMU Panoptic dataset; showing comparison with state-of-the-art method viewLSTM [9] with single-view input setup. We show two samples and the resolution is 56×56 .

a maximum of 72 views for training and testing. We examine the impact of number of training videos on the quality of synthesized videos and compare with SOTA.

Large-scale Multiview Experiment. In this setup, we used 72 camera viewpoints. Specifically, we select 3 panels (Number 4, 5 and 17) and use all 24 views from each panel, totalling 72 views. We use 56 viewpoints for training, and 16 viewpoints for the testing with a split of 6,244 training and 1,132 test samples. Training with so many viewpoints can be challenging due to computation cost. So for each iteration we randomly selected, six views from one of the panels, five input views and a query view. Testing followed a similar setup. For each panel, we fix the input viewpoints from view 1 to view 5 *i.e.* (v_1, v_2, v_3, v_4, v_5) and test on the remaining 19 viewpoints *i.e.* the query view points are from v_6 to v_{24} . SSIM [19] and PSNR for frame quality evaluation and Fréchet Video Distance (FVD) [20] to measure the video quality.

Table 4 shows that the proposed method is successful at synthesizing high quality video clips from multiple query views. Owing to the weight sharing nature of the proposed approach, we are able to change the number of testing input clips irrespective of training. Figure 1 shows qualitative results with two fixed input views and for different query views. The predicted video frames capture the motion and viewpoints correctly.

Table 1. Quantitative results for Large-scale Multiview experiment (72 views), averaged over 19 query views of each of the three panels of CMU Panoptic at 56×56 resolution. Views (v_1, v_2, v_3, v_4, v_5) are input views and views v_6 to v_{24} are query (output) views.

Panels	Metrics		
	SSIM(\uparrow)	PSNR(\uparrow)	FVD(\downarrow)
4	0.837	25.15	11.52
5	0.848	24.9	13.42
17	0.845	25.46	13.31

Comparison with state-of-the-art

We compare our results with a video based method viewLSTM [9] which uses skeleton prior from the query view and a frame-based method SynSin [21], both trained from scratch. For training, we use three viewpoints, however for a fair comparison with baselines (use one input view), we tested our network employing a single input view setup. Table 6 shows comparison between these methods in terms of SSIM, PSNR and FVD scores. As shown in Table 6, we report 26.1%, 13.6% and 60% improvement in SSIM, PSNR and FVD scores respectively over viewLSTM [9], for clips length $T=16$. Similar improvements are observed when compared with SynSin [21] quantitatively. For visual comparison, some video frames are shown in Figure 3. Our

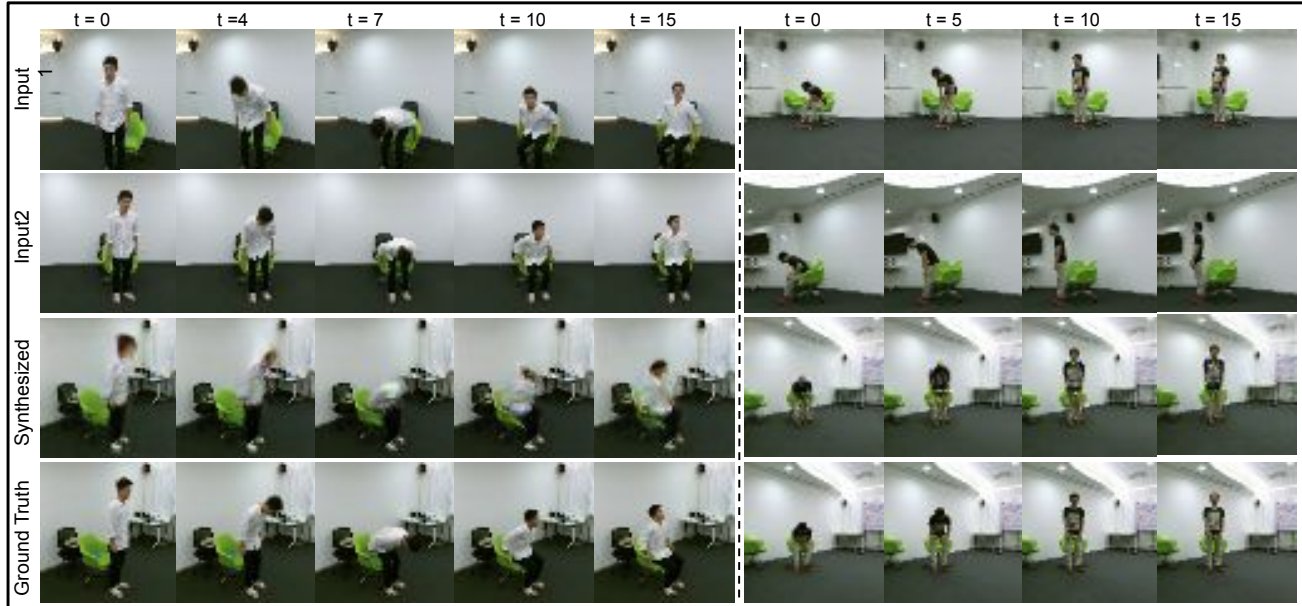


Fig. 4. Qualitative results on NTU-RGB+D Dataset [11] with multi-input view setup, resolution 56×56 . The first two rows show clips from input views v_1 and v_2 . The synthesized output from the query view v_q is shown in the third row followed by the corresponding ground truth frames on the last row.

Table 2. Quantitative comparison of our method with state-of-the-art on CMU Panoptic dataset at 56×56 resolution for different lengths of synthesized video frames.

Methods	Metrics					
	SSIM(\uparrow)				PSNR(\uparrow)	FVD(\downarrow)
	T=16	T=24	T=32	T=48	T=16	T=16
[9]	0.681	0.667	0.588	0.488	22.96	22.87
[21]	0.744	0.752	0.748	0.735	21.53	17.62
Ours	0.859	0.834	0.809	0.782	26.08	9.15

model is able to get better quality (sharpness), colors, motion as well as background details. Although, there is ample scope of improvement as compared to ground truth, finer details are much more formed with the proposed approach.

4.3. Novel View Video Prediction: NTU-RGB+D

Since the NTU-RGB+D dataset [11] consists of three camera viewpoints, our experiment uses two views as input and the third view as query. Qualitative results along with the ground truth are visualized in Figure 4. Consistent with SSIM and PSNR values Table 7 (Proposed), the network is able to synthesize the persons in the frames as well as the background details of the query viewpoint correctly. We show frames at three different time steps and observe that the synthesized frames are able to capture the motion similar to the ground truth which is also supported by low FVD scores. As ablations studies, we evaluate the role of global and view-

Table 3. SSIM, PSNR and FVD scores for Network Ablations on NTU-RGB+D Dataset [11] using View Dependent (VD) stream, Global Representation (GR) stream and the Full model (Full) on 56×56 resolution with multi-view input setup. The table shows the average scores for all input-output view combinations.

Networks	Metrics		
	SSIM(\uparrow)	PSNR(\uparrow)	FVD(\downarrow)
VD (tested)	0.335	12.58	18.93
GR (tested)	0.639	17.45	15.68
VD (trained)	0.563	16.22	16.77
GR (trained)	0.792	20.05	13.45
Proposed	0.817	20.77	12.31

dependent blocks separately. First we test the fully trained network by using one block at a time and call them VD(tested) and GR(tested). Secondly, we train both blocks separately and call VD(trained) and GR(trained). The results are shown in Table 7 confirming the effect of the two blocks together produces better output.

5. CONCLUSION

We propose a novel approach for unseen view video prediction via a dual representation. The dual representation comprises of global and view dependent representations which enables novel view video prediction. The proposed approach takes single/multiple clips as input for video prediction from

the novel view without any priors. Using only RGB videos, our evaluation on two real world datasets shows an improvement over state-of-the-art.

6. REFERENCES

- [1] Steven M Seitz and Charles R Dyer, “Physically-valid view synthesis by image interpolation,” in *Proceedings IEEE Workshop on Representation of Visual Scenes (In Conjunction with ICCV’95)*. IEEE, 1995, pp. 18–25.
- [2] Ismael Daribo and Béatrice Pesquet-Popescu, “Depth-aided image inpainting for novel view synthesis,” in *2010 IEEE International workshop on multimedia signal processing*. IEEE, 2010, pp. 167–170.
- [3] Tinghui Zhou, Shubham Tulsiani, Weilun Sun, Jitendra Malik, and Alexei A Efros, “View synthesis by appearance flow,” in *European conference on computer vision*. Springer, 2016, pp. 286–301.
- [4] Kyle Olszewski, Sergey Tulyakov, Oliver Woodford, Hao Li, and Linjie Luo, “Transformable bottleneck networks,” in *Proceedings of the IEEE International Conference on Computer Vision*, 2019, pp. 7648–7657.
- [5] Vincent Sitzmann, Michael Zollhöfer, and Gordon Wetzstein, “Scene representation networks: Continuous 3d-structure-aware neural scene representations,” in *Advances in Neural Information Processing Systems*, 2019, pp. 1119–1130.
- [6] Carl Vondrick, Hamed Pirsiavash, and Antonio Torralba, “Generating videos with scene dynamics,” in *Advances In Neural Information Processing Systems*, 2016, pp. 613–621.
- [7] Sergey Tulyakov, Ming-Yu Liu, Xiaodong Yang, and Jan Kautz, “Mocogan: Decomposing motion and content for video generation,” in *Proceedings of the IEEE conference on computer vision and pattern recognition*, 2018, pp. 1526–1535.
- [8] Simone Palazzo, Concetto Spampinato, P D’Oro, Daniela Giordano, and Mubarak Shah, “Generating synthetic video sequences by explicitly modeling object motion,” in *Proceedings of the European Conference on Computer Vision (ECCV)*, 2018, pp. 0–0.
- [9] Mohamed Ilyes Lakhall, Oswald Lanz, and Andrea Cavallaro, “View-1stm: Novel-view video synthesis through view decomposition,” in *Proceedings of the IEEE International Conference on Computer Vision*, 2019, pp. 7577–7587.
- [10] Hanbyul Joo, Hao Liu, Lei Tan, Lin Gui, Bart Nabbe, Iain Matthews, Takeo Kanade, Shohei Nobuhara, and Yaser Sheikh, “Panoptic studio: A massively multiview system for social motion capture,” in *Proceedings of the IEEE International Conference on Computer Vision*, 2015, pp. 3334–3342.
- [11] Amir Shahroudy, Jun Liu, Tian-Tsong Ng, and Gang Wang, “Ntu rgb+ d: A large scale dataset for 3d human activity analysis,” in *Proceedings of the IEEE conference on computer vision and pattern recognition*, 2016, pp. 1010–1019.
- [12] Eddie Cooke, Peter Kauff, and Thomas Sikora, “Multi-view synthesis: A novel view creation approach for free viewpoint video,” *Signal Processing: Image Communication*, vol. 21, no. 6, pp. 476–492, 2006.
- [13] Stephen Lombardi, Tomas Simon, Jason Saragih, Gabriel Schwartz, Andreas Lehrmann, and Yaser Sheikh, “Neural volumes: Learning dynamic renderable volumes from images,” *arXiv preprint arXiv:1906.07751*, 2019.
- [14] M Domański, M Gotfryd, and K Wegner, “View synthesis for multiview video transmission,” .
- [15] Mohamed Ilyes Lakhall, Davide Boscaini, Fabio Poiesi, Oswald Lanz, and Andrea Cavallaro, “Novel-view human action synthesis,” *arXiv preprint arXiv:2007.02808*, 2020.
- [16] Joao Carreira and Andrew Zisserman, “Quo vadis, action recognition? a new model and the kinetics dataset,” in *proceedings of the IEEE Conference on Computer Vision and Pattern Recognition*, 2017, pp. 6299–6308.
- [17] Karen Simonyan and Andrew Zisserman, “Very deep convolutional networks for large-scale image recognition,” *arXiv preprint arXiv:1409.1556*, 2014.
- [18] Ian Goodfellow, Jean Pouget-Abadie, Mehdi Mirza, Bing Xu, David Warde-Farley, Sherjil Ozair, Aaron Courville, and Yoshua Bengio, “Generative adversarial nets,” in *Advances in neural information processing systems*, 2014, pp. 2672–2680.
- [19] Zhou Wang, Alan C Bovik, Hamid R Sheikh, and Eero P Simoncelli, “Image quality assessment: from error visibility to structural similarity,” *IEEE transactions on image processing*, vol. 13, no. 4, pp. 600–612, 2004.
- [20] Thomas Unterthiner, Sjoerd van Steenkiste, Karol Kurach, Raphael Marinier, Marcin Michalski, and Sylvain Gelly, “Towards accurate generative models of video: A new metric & challenges,” *arXiv preprint arXiv:1812.01717*, 2018.
- [21] Olivia Wiles, Georgia Gkioxari, Richard Szeliski, and Justin Johnson, “Synsin: End-to-end view synthesis

from a single image,” in *IEEE/CVF Conference on Computer Vision and Pattern Recognition (CVPR)*, June 2020.

- [22] J Deng, W Dong, R Socher, LJ Li, K Li, and L Imagenet Fei-Fei, “A large-scale hierarchical image database. computer vision and pattern recognition, 2009. cvpr 2009,” in *IEEE Conference on*, pp. 248–255.
- [23] Mohamed Ilyes Lakhhal, Oswald Lanz, and Andrea Cavallaro, “Pose guided human image synthesis by view disentanglement and enhanced weighting loss,” in *Proceedings of the European Conference on Computer Vision (ECCV)*, 2018, pp. 0–0.
- [24] Liqian Ma, Xu Jia, Qianru Sun, Bernt Schiele, Tinne Tuytelaars, and Luc Van Gool, “Pose guided person image generation,” in *Advances in Neural Information Processing Systems*, 2017, pp. 406–416.
- [25] Kaiming He, Xiangyu Zhang, Shaoqing Ren, and Jian Sun, “Deep residual learning for image recognition,” 2015.

NOVEL VIEW VIDEO PREDICTION USING A DUAL REPRESENTATION

SUPPLEMENTARY MATERIAL

Sarah Shiraz, Krishna Regmi, Shruti Vyas, Yogesh S. Rawat, Mubarak Shah
Center for Research in Computer Vision (CRCV), University of Central Florida

7. ADDITIONAL NETWORK DETAILS

Video encoder is a modified I3D network[16] where the modifications are: (i) remove max pooling layer after block 2, (ii) for max pooling in block 3 & 4, stride is set to $2 \times 1 \times 1$, (iii) Add $1 \times 1 \times 1$ convolutional layer before average pooling, to reduce the number of feature maps to 256. Finally, V_E is initialized with I3D weights pre-trained on ImageNet[22].

View Embedder, VE is a trilinear interpolation layer which takes the view information (v_i or v_q) of size $(1 \times 1 \times d)$, where, d is the number of view dimensions, and interpolates the spatial size to match with that of the encoder features in case of the View Dependent Block and the Global Representation Block (i.e. v_i and $v_i - v_q$) and convLSTM features in the case of Video Decoder (v_q) respectively, as we can see from the Network Diagram in the manuscript.

View Dependent Block, V_T consists of two fully-connected layers of size $d^p \times d^p$ and $2d^p \times d^p$ where d^p is the number of view dimensions in v_i^p or v_q^p . Next, it uses a bidirectional convLSTM with $64 \ 3 \times 3 \times 3$ kernels; followed by a unidirectional convLSTM with $128 \ 3 \times 3 \times 3$ filters in the convolutions. The output features from the Video Encoder, e'_i and the relative view embeddings from the View Embedder are concatenated channelwise and passed as input to this block.

Global Representation Block also consists of a bidirectional convLSTM followed by a unidirectional convLSTM. Here, the first convLSTM consists of $128 \ 3 \times 3 \times 3$ filters whereas the second one uses $256 \ 3 \times 3 \times 3$ filters.

Query Network is a single-layer convolutional network with 256 filters and filter size of $5 \times 5 \times 5$.

Video Decoder has 8 convolutional layers (combined with upsampling layers) with kernel sizes $5 \times 5 \times 5$ and 256, 256, 256, 128, 64, 3 filters respectively. The second last layer uses kernel size $3 \times 3 \times 3$. The final layer is the Tanh activation.

Discriminator is a 6-layered 3D CNN with $3 \times 3 \times 3$ kernels and strides of $2 \times 2 \times 2$. The number of filters in each layer is [16, 32, 64, 128, 256, 256] respectively. After the last convolution, we add a fully connected layer followed by

Sigmoid activation.

8. ADDITIONAL RESULTS

8.1. CMU Panoptic Dataset [10]

Large-scale Multiview Experiment. We provide additional qualitative results on CMU Panoptic Dataset.

Figure 5 depicts the frames at time $t = 0, 8$ and 15 for five input views as well as the synthesized frames and the corresponding ground truth frames from the query view.

The detailed quantitative evaluation is provided in Table 4. The evaluation is conducted per panel separately. For each panel, the viewpoints from v_1 to v_5 are fixed as input views and the output video clips for the remaining 19 viewpoints (v_6 to v_{24}) are synthesized. The SSIM, PSNR and FVD scores are provided in Table 4. The average scores for panel 4, 5 and 17 are

For the same configuration, we provide additional qualitative results in Figure 7 for randomly selected query views from the pool of viewpoints from v_6 to v_{24} . It can be observed that video frames and motion are equally good for each of the query views given the five input views as shown.

Effect of Multiple Input Views.

This analysis is conducted to understand the impact of multiple input views on the quality of the synthesized videos. The number of input clips is increased from 1 to 5 to synthesize the video from the query view and report the results in Figure 6. As expected, with an increase in the number of input views the video quality improves. This validates that the network is able to capture and aggregate the features pertinent to each view and exploit them to synthesize the query view.

The SSIM and PSNR scores are reported for the synthesized video frames in Table 5. The input and query views are selected from Panel 4 for this analysis. We observe that the scores improve as the number of input view increases from single to multiple views. This is possible since the multiple input views are successful at providing greater scene details useful to learn to synthesize the query view.

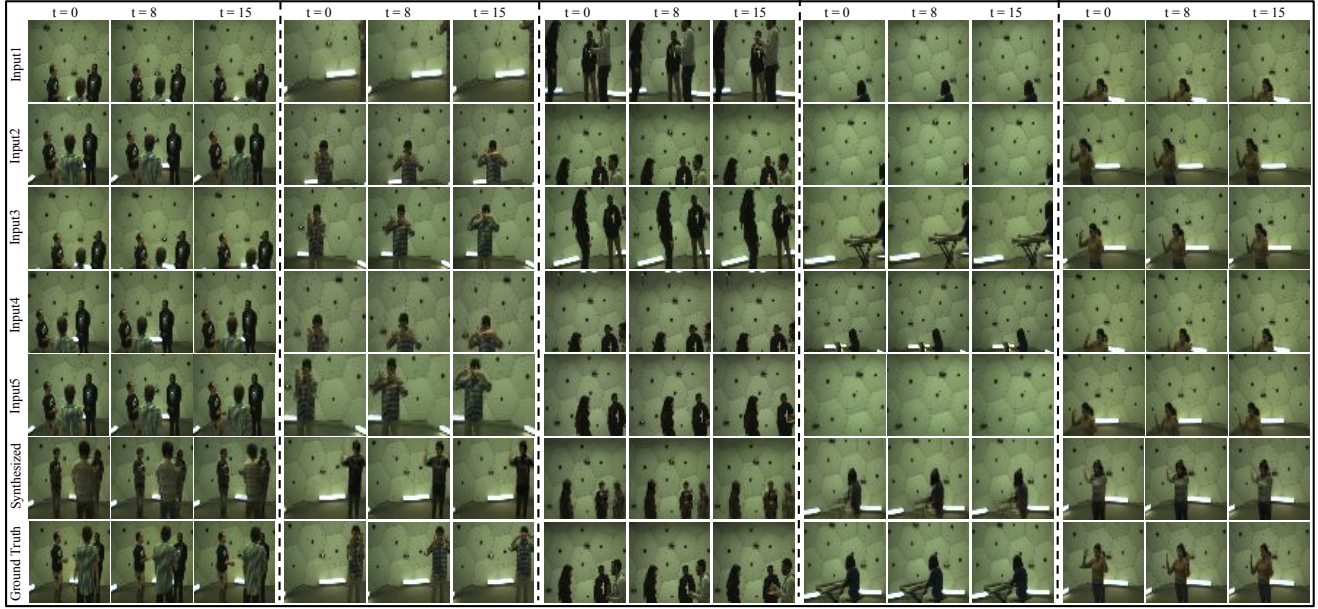


Fig. 5. Qualitative results on CMU Panoptic dataset for 72 views experiment with five input views showing three different samples. The resolution is 56×56 .

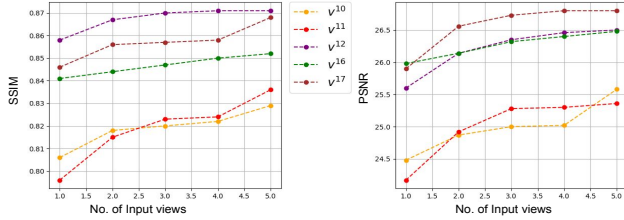


Fig. 6. SSIM and PSNR scores vs the number of input views. Higher number of views help better prediction quality. The plots show scores for 5 randomly chosen query views.

Higher Resolution Experiment For the same setup, we also conduct experiment on 224×224 resolution. The qualitative results are shown in Figure 8. The model is able to preserve fine details and produce sharper frames with an SSIM and PSNR score of 0.812 and 24.55, respectively.

Comparison with viewLSTM[9]. Here, we provide additional qualitative and quantitative evaluation of our proposed approach with state-of-the-art viewLSTM [9] in Figure 9 and Table 6 respectively. The experimental details are provided in the manuscript in Section 5.1.

In Figure 9, we show three samples from different input viewpoints, each at three time instances, $t = 0, 8$ and 15 . The actors in the images are performing different actions. Qualitatively, our proposed method is successful at synthesizing better images with sharper foreground-background boundaries

and also capture the motion of the person along the temporal sequence.

The detailed quantitative result in Table 6 provides the performance of our method and the state-of-the-art viewLSTM [9] for view transformation between the Panels 2,4 and 10 (Node 10). The SOTA method uses the query view skeleton priors to synthesize the query RGB frames, whereas our method doesn't utilize the skeleton information from the query view. We observe that our proposed method outperforms the existing SOTA by huge margins for all evaluation metrics.

8.2. NTU-RGB+D Dataset [11]

Refer Section 4.2 in the manuscript for the summarized quantitative analysis on network ablations. Here, we provide the detailed network and loss ablation in terms of quantitative results and qualitative visualizations on NTU-RGB+D Dataset along with the comparison with existing works.

Network Ablations. We performed two types of ablations for evaluating the role of the global and view-dependent representations. First, we tested the fully trained network by using only one representation at a time. Figure 10 shows the testing results with global representation r_g and/or view-dependent representation r_t . With global representation r_g , the foreground and background are almost formed however view-dependent representation r_t is not meaningful alone. The r_t helps by filling in the view specific finer details and only makes sense along with the global representation. It is visibly

Table 4. Quantitative results (SSIM, PSNR and FVD scores) for 72 views experiment on CMU Panoptic dataset on 56×56 resolution. For each panel, input views are fixed to $(v_1, v_2, v_3, v_4, v_5)$ and we test output views from v_6 to v_{24} .

Query View	Panel 4			Panel 5			Panel 17		
	SSIM(\uparrow)	PSNR(\uparrow)	FVD(\downarrow)	SSIM(\uparrow)	PSNR(\uparrow)	FVD(\downarrow)	SSIM(\uparrow)	PSNR(\uparrow)	FVD(\downarrow)
v_6	0.814	24.46	7.58	0.852	26.79	11.79	0.855	25.94	11.80
v_7	0.795	24.56	11.64	0.843	25.66	13.17	0.820	26.06	13.17
v_8	0.794	24.02	10.49	0.842	25.94	16.01	0.834	26.15	16.04
v_9	0.813	24.7	10.66	0.827	25.16	17.65	0.795	25.18	14.23
v_{10}	0.829	25.58	10.91	0.828	24.99	14.80	0.807	25.69	14.82
v_{11}	0.836	25.36	11.98	0.823	24.21	12.72	0.809	24.33	12.67
v_{12}	0.871	26.50	8.24	0.807	23.17	10.92	0.784	24.17	10.89
v_{13}	0.834	25.09	10.80	0.832	23.61	13.33	0.805	24.62	13.32
v_{14}	0.811	24.17	15.01	0.808	23.26	11.86	0.789	24.25	11.85
v_{15}	0.827	24.7	8.24	0.844	24.43	16.60	0.797	23.90	16.60
v_{16}	0.852	26.48	12.69	0.860	25.06	10.84	0.813	24.62	10.87
v_{17}	0.868	26.80	11.01	0.835	23.76	10.50	0.808	24.31	10.48
v_{18}	0.846	27.43	10.44	0.817	24.82	9.86	0.810	24.14	9.84
v_{19}	0.829	25.01	12.25	0.836	23.90	13.71	0.816	24.60	13.70
v_{20}	0.820	25.02	13.26	0.851	25.68	13.97	0.827	24.95	13.97
v_{21}	0.822	25.06	12.14	0.811	24.60	14.91	0.832	25.83	14.89
v_{22}	0.810	24.82	10.08	0.839	24.44	15.04	0.804	24.65	15.04
v_{23}	0.824	25.15	15.53	0.839	24.73	14.05	0.811	24.66	14.02
v_{24}	0.835	25.61	15.94	0.823	23.65	13.31	0.750	20.59	14.70

obvious that best results are obtained with the dual representation r . The detailed quantitative evaluation for single and multi-input setup is shown in Table 7 (Row 1-2).

Secondly, we trained the network with only one representation at a time to investigate the impact of each branch in our architecture. To examine the role of View Dependent block, we employ View Dependent block V_T , in conjunction with Video Encoder V_E , and Video Decoder V_D (i.e. Global Representation block V_G is removed). To examine the role of Global Representation block, we employ Global Representation block V_G , in conjunction with Video Encoder V_E , and Video Decoder V_D (i.e. View Dependent block V_T is removed).

The final experiment is performed on the full model *i.e.* V_T and V_G combined. The qualitative results for network ablations are presented in Figure 11. The first row shows the frames from input clip, followed by the synthesized outputs for View Dependent (VD) stream, Global Representation (GR) stream and the full model in rows two, three and four respectively. Finally, the ground truth frames are shown in the last row. The outputs from the network with View Dependent stream contains visible artifacts in the frames. The network with Global Representation stream shows improvements in visual quality of the output over the network with View Dependent branch only. Finally, the full model is able to add finer details like arm and leg (Figure 11, right panel) in the synthesized output.

Table 7 (Row 3-4) shows detailed quantitative results for network ablations for single and multiple input-view settings. The quantitative results are consistent for both single and mul-

iple input-view setups, and for all input and output view combinations. The results show that View Dependent and Global Representation streams learn complementary features that are aggregated by the full model (Table 7 Row 5) and generate better results.

Comparison with Existing Works.

In order to compare with the existing novel view prediction methods, we test our network to synthesize a query view video using a single view video as input. We input multiple copies of the same input clip, as explained earlier with CMU Panoptic dataset. The experiment is conducted at 112×112 resolution. We compare with a state-of-the-art video-based method, viewLSTM [9] and two frame-based methods [23, 24].

The quantitative comparison is shown in Table 9. It can be observed that SSIM with proposed approach is comparable to ViewLSTM [9], without using any priors from the query view. ViewLSTM [9], on the other hand, uses multiple priors from the query view, i.e both depth and skeleton information. The frame-based methods [23, 24] were reportedly trained to predict smaller view-point changes. When trained on NTU-RGB+D there are larger view point changes and our method predicts better quality videos. Also, these methods are unable to capture the temporal coherency between the synthesized frames.

Figure 13 shows a qualitative comparison between the outputs synthesized by viewLSTM [9] (second row) and our proposed method (third row) on NTU-RGB+D dataset. The samples are shown for three time steps and for two samples. As seen with the SSIM scores, our method produces sharper

Table 5. SSIM and PSNR scores for investigating the effect of varying the number of input views. We randomly select 9 query views v_k from panel 4 and increase the input views from 1 to 5.

Metrics	Query View	Input Views				
	v_k	(v_1)	(v_1, v_2)	(v_1, v_2, v_3)	(v_1, v_2, v_3, v_4)	$(v_1, v_2, v_3, v_4, v_5)$
SSIM(\uparrow)	v_6	0.789	0.803	0.808	0.812	0.814
	v_{10}	0.806	0.818	0.820	0.822	0.829
	v_{11}	0.796	0.815	0.823	0.824	0.836
	v_{12}	0.858	0.867	0.870	0.871	0.871
	v_{13}	0.807	0.816	0.820	0.819	0.834
	v_{14}	0.776	0.781	0.784	0.784	0.811
	v_{16}	0.841	0.844	0.847	0.850	0.852
	v_{17}	0.846	0.856	0.857	0.858	0.868
	v_{20}	0.786	0.797	0.809	0.812	0.820
PSNR(\uparrow)	v_6	23.51	24.06	24.27	24.41	24.46
	v_{10}	24.48	24.87	25.00	25.02	25.58
	v_{11}	24.17	24.92	25.28	25.30	25.36
	v_{12}	25.60	26.14	26.35	26.46	26.50
	v_{13}	24.82	25.16	25.25	25.22	25.09
	v_{14}	23.34	23.54	23.63	23.80	24.17
	v_{16}	25.98	26.14	26.32	26.40	26.48
	v_{17}	25.90	26.56	26.73	26.80	26.80
	v_{20}	23.99	24.29	24.64	24.83	25.02

Table 6. Quantitative comparison with state-of-the-art viewLSTM[9] on CMU Panoptic dataset at 56×56 resolution and single-input setup. Our method performs significantly better than SOTA viewLSTM[9] on all three evaluation metrics for all input-output view combinations.

Method	Metrics	Input View \rightarrow Output View						Average Score
		$v_1 \rightarrow v_2$	$v_1 \rightarrow v_3$	$v_2 \rightarrow v_1$	$v_2 \rightarrow v_3$	$v_3 \rightarrow v_1$	$v_3 \rightarrow v_2$	
[9]	SSIM (\uparrow)	0.675	0.684	0.686	0.673	0.690	0.680	0.681
	PSNR (\uparrow)	23.03	23.16	22.56	23.07	22.69	23.24	22.96
	FVD (\downarrow)	22.43	25.67	20.62	25.73	20.32	22.48	22.87
[21]	SSIM (\uparrow)	0.740	0.751	0.753	0.748	0.742	0.732	0.744
	PSNR (\uparrow)	21.33	21.75	22.53	21.41	21.44	20.70	21.53
	FVD (\downarrow)	18.23	18.98	16.23	17.95	17.88	16.42	17.62
Ours	SSIM (\uparrow)	0.862	0.853	0.852	0.861	0.858	0.876	0.859
	PSNR (\uparrow)	26.37	25.48	25.85	25.58	26.34	26.87	26.08
	FVD (\downarrow)	8.51	10.12	9.21	9.98	8.93	8.20	9.15

Table 7. SSIM, PSNR and FVD scores for Network Ablations on NTU-RGB+D Dataset [11] using View Dependent (VD) stream, Global Representation (GR) stream and the full model (Full) on 56×56 resolution. The left panel shows the results for multi-input view setup, whereas the right panel shows single-input view setup results.

Network	Metric	Multi-Input Setup			Avg Score	Single Input Setup						Avg Score
		$(v_1, v_2) \rightarrow v_3$	$(v_2, v_3) \rightarrow v_1$	$(v_1, v_3) \rightarrow v_2$		$v_1 \rightarrow v_2$	$v_1 \rightarrow v_3$	$v_2 \rightarrow v_1$	$v_2 \rightarrow v_3$	$v_3 \rightarrow v_1$	$v_3 \rightarrow v_2$	
VD(tested)	SSIM(\uparrow)	0.313	0.352	0.340	0.335	0.323	0.327	0.329	0.316	0.315	0.323	0.323
	PSNR(\uparrow)	12.67	13.20	11.88	12.58	12.09	12.52	12.59	11.92	11.89	12.11	12.18
	FVD(\downarrow)	18.20	18.48	18.03	18.23	19.23	19.93	18.96	18.92	17.78	17.67	18.74
GR(tested)	SSIM(\uparrow)	0.634	0.647	0.637	0.639	0.634	0.627	0.629	0.624	0.628	0.631	0.629
	PSNR(\uparrow)	17.23	17.72	17.40	17.45	16.12	16.96	16.66	17.02	16.67	16.31	16.62
	FVD(\downarrow)	15.45	15.82	15.76	15.68	15.39	15.87	16.02	16.28	16.71	15.39	15.94
VD(trained)	SSIM(\uparrow)	0.548	0.579	0.563	0.563	0.539	0.517	0.548	0.547	0.537	0.519	0.534
	PSNR(\uparrow)	16.13	16.21	16.32	16.22	15.86	15.62	15.59	15.59	15.63	15.747	15.67
	FVD(\downarrow)	16.84	16.57	16.92	16.77	17.48	17.37	16.77	17.11	16.90	17.47	17.18
GR(trained)	SSIM(\uparrow)	0.783	0.814	0.780	0.792	0.781	0.777	0.804	0.774	0.799	0.773	0.784
	PSNR(\uparrow)	19.99	20.67	19.50	20.05	19.56	19.83	20.2	19.67	20.04	19.23	19.755
	FVD(\downarrow)	13.25	13.54	13.57	13.45	13.69	13.17	12.12	13.78	13.17	13.89	13.33
Full	SSIM(\uparrow)	0.801	0.834	0.805	0.813	0.804	0.793	0.828	0.783	0.815	0.790	0.802
	PSNR(\uparrow)	20.65	21.40	20.34	20.79	20.44	20.48	20.97	20.17	20.63	20.02	20.45
	FVD(\downarrow)	12.75	11.25	12.93	12.31	11.01	11.04	11.76	12.78	11.94	12.28	11.80

Table 8. SSIM and PSNR scores for different combination of losses on NTU Dataset[11] 56×56 resolution. L_2 is the Reconstruction loss, L_p is the Perceptual loss and L_{adv} is the Adversarial loss. The left panel shows the results for multi-input view setup, whereas the right panel shows single-input view setup results.

Metrics	Losses			Multi-Input Setup			Avg Score	Single-Input Setup						Avg Score
	L_2	L_p	L_{adv}	$(v_1, v_2) \rightarrow v_3$	$(v_2, v_3) \rightarrow v_1$	$(v_1, v_3) \rightarrow v_2$		$v_1 \rightarrow v_2$	$v_1 \rightarrow v_3$	$v_2 \rightarrow v_1$	$v_2 \rightarrow v_3$	$v_3 \rightarrow v_1$	$v_3 \rightarrow v_2$	
SSIM (\uparrow)	✓			0.699	0.723	0.704	0.708	0.689	0.704	0.653	0.678	0.651	0.670	0.674
		✓	✓	0.737	0.775	0.745	0.752	0.703	0.714	0.601	0.710	0.662	0.662	0.675
	✓	✓		0.791	0.833	0.796	0.806	0.773	0.774	0.778	0.768	0.766	0.749	0.768
	✓		✓	0.784	0.825	0.789	0.799	0.783	0.776	0.798	0.761	0.815	0.787	0.786
	✓	✓	✓	0.801	0.834	0.805	0.813	0.804	0.793	0.828	0.783	0.815	0.790	0.802
PSNR (\uparrow)	✓			17.56	18.55	17.89	18.00	17.25	18.27	16.92	17.27	16.55	17.01	17.21
		✓	✓	18.96	19.94	18.78	19.22	17.85	18.464	15.82	18.39	17.34	17.34	17.53
	✓	✓		19.69	21.63	20.38	20.72	19.76	20.24	19.72	18.03	19.31	18.93	19.29
	✓		✓	20.19	21.06	19.91	20.38	19.76	20.00	20.15	18.58	19.55	18.8	19.47
	✓	✓	✓	20.65	21.40	20.34	20.79	20.44	20.48	20.97	20.17	20.63	20.02	20.45

Table 9. SSIM scores comparison with existing frame based methods[23, 24] and state-of-the-art video-based method, viewLSTM [9] on **NTU-RGB+D dataset at 112×112 resolution** with single-view input setup. The scores for viewLSTM [9] are computed for the videos synthesized using both depth and skeleton priors from the query view.

Metric	Methods			
	[23]	[24]	[9]	Ours
SSIM(\uparrow)	0.554	0.560	0.783	0.791

Table 10. SSIM, PSNR and FVD scores for different combination of losses on NTU-RGB+D Dataset [11] on 56×56 resolution.

Losses			Metrics		
L_2	L_p	L_{adv}	SSIM(\uparrow)	PSNR(\uparrow)	FVD(\downarrow)
✓			0.708	18.00	15.42
	✓	✓	0.752	19.22	13.96
✓	✓		0.806	20.72	13.28
✓		✓	0.799	20.38	13.76
✓	✓	✓	0.817	20.77	12.31

foreground objects and better background details.

We provide more qualitative results comparing with our baselines VGD [23], PG² [24], ResNet [25] and viewLSTM [9] in Figure 12. As can be seen, the frame-bases baselines VDG and PG² are not able to produce even the scene structure correctly. ResNet, which is used as a video-based baseline, generates correct scene structure but has visible artifacts present. VNet produces better results but the video quality is low. Finally, we can observe that the proposed method perfectly generates the background as well as the actor performing the action with better motion as well.

Loss Ablations. Figure 14 shows the qualitative results obtained by employing different losses. Using only the reconstruction loss produces very blurry results. Adversarial and perceptual loss combined ($L_p + L_{adv}$) helps in sharpening the frames but does not get the color information and background correctly. Adding perceptual loss with reconstruction loss ($L_2 + L_p$) gets the background information well, but the structures of bodies are not defined. $L_2 + L_{adv}$ also produces sharp results with correct background but lacks in producing correct body structures. Finally, combining $L_2 + L_p + L_{adv}$, we get improved results compared to other losses.

Table 8 shows detailed quantitative results for loss ablations for single input-view settings. The results are consistent for different input and output view combinations. The use of all three losses helps to synthesize query view outputs better than using only one or two loss combinations as validated by the table.

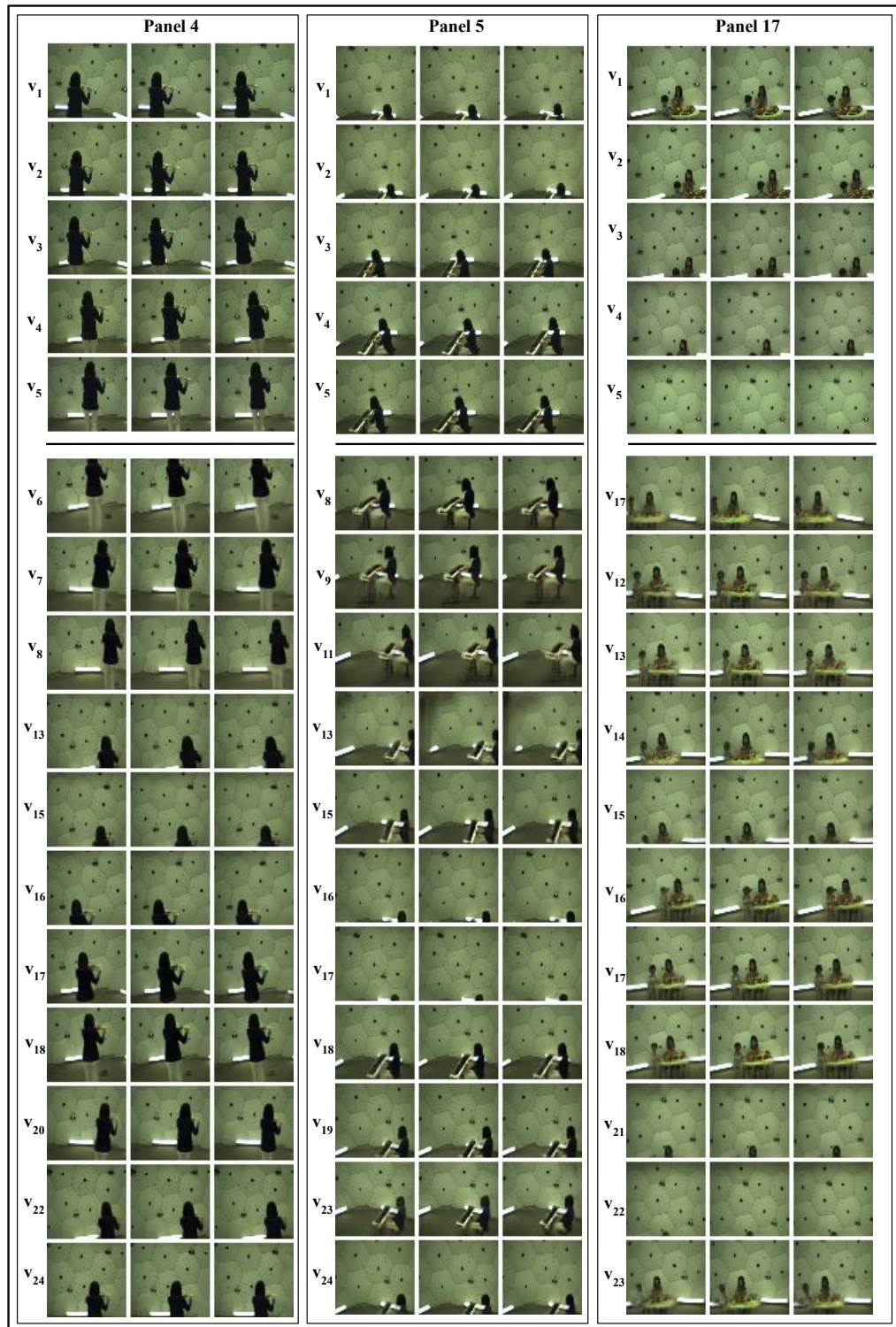


Fig. 7. Qualitative Results on CMU Panoptic dataset showing synthesized frames employing five input views (v_1 through v_5) and randomly selected query views from the remaining views ($v_6 - v_{24}$) for each panel. We show 3 samples and the resolution is 56×56 .

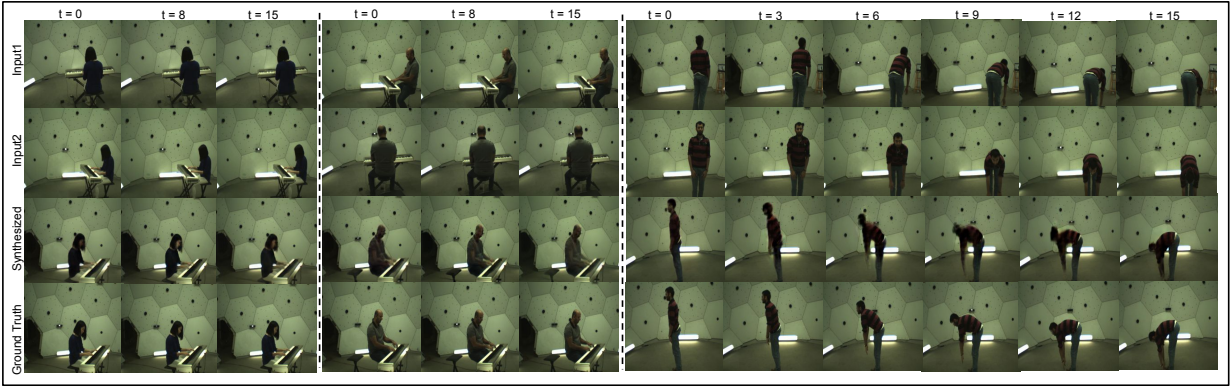


Fig. 8. Qualitative Results on CMU Panoptic dataset with multi-view input setup. We show three samples and the resolution is 224×224 .

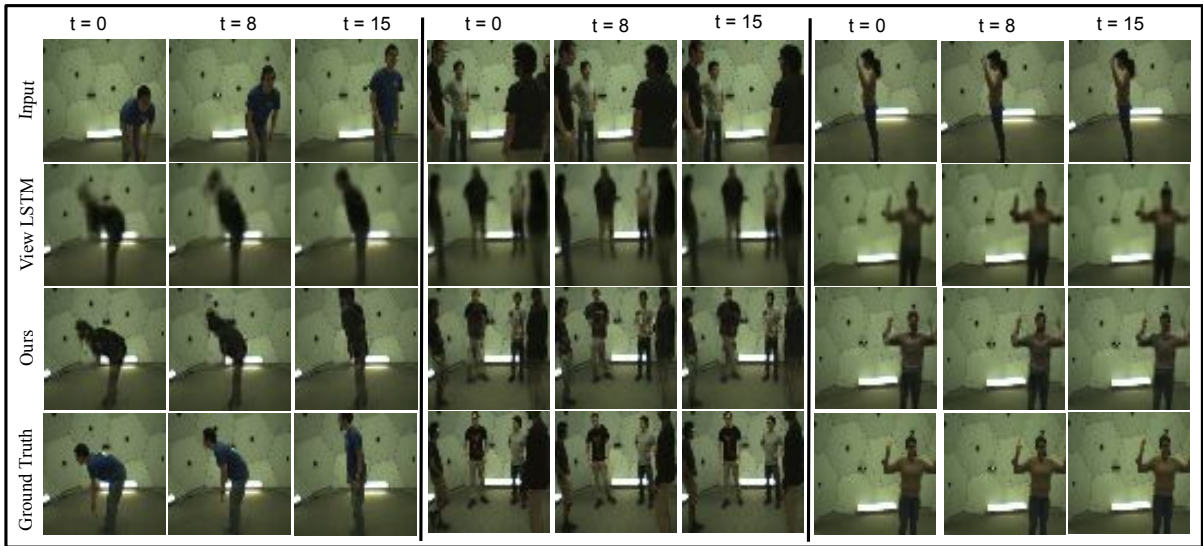


Fig. 9. Qualitative Results showing the comparison of our proposed method with state-of-the-art method viewLSTM [9] on CMU Panoptic dataset. We show 3 samples, each with frames at time $t=0, 8$ and 15 ; and the resolution is 56×56 .



Fig. 10. Qualitative results showing Network Ablations on two samples of NTU-RGB+D Dataset [11], showing the comparison between View Dependent (tested), Global Representation (tested) and Full Model at 56×56 resolution for multiple input view setup.

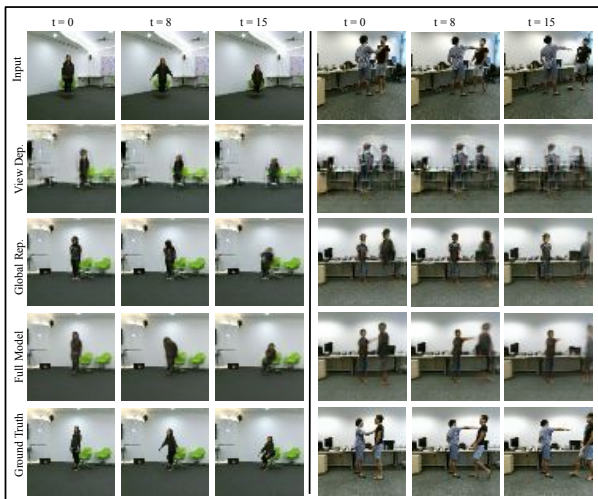


Fig. 11. Qualitative results showing Network Ablations on two samples of NTU-RGB+D Dataset [11], showing the comparison between View Dependent (trained), Global Representation (trained) and Full Model at 56×56 resolution for single input view setup.

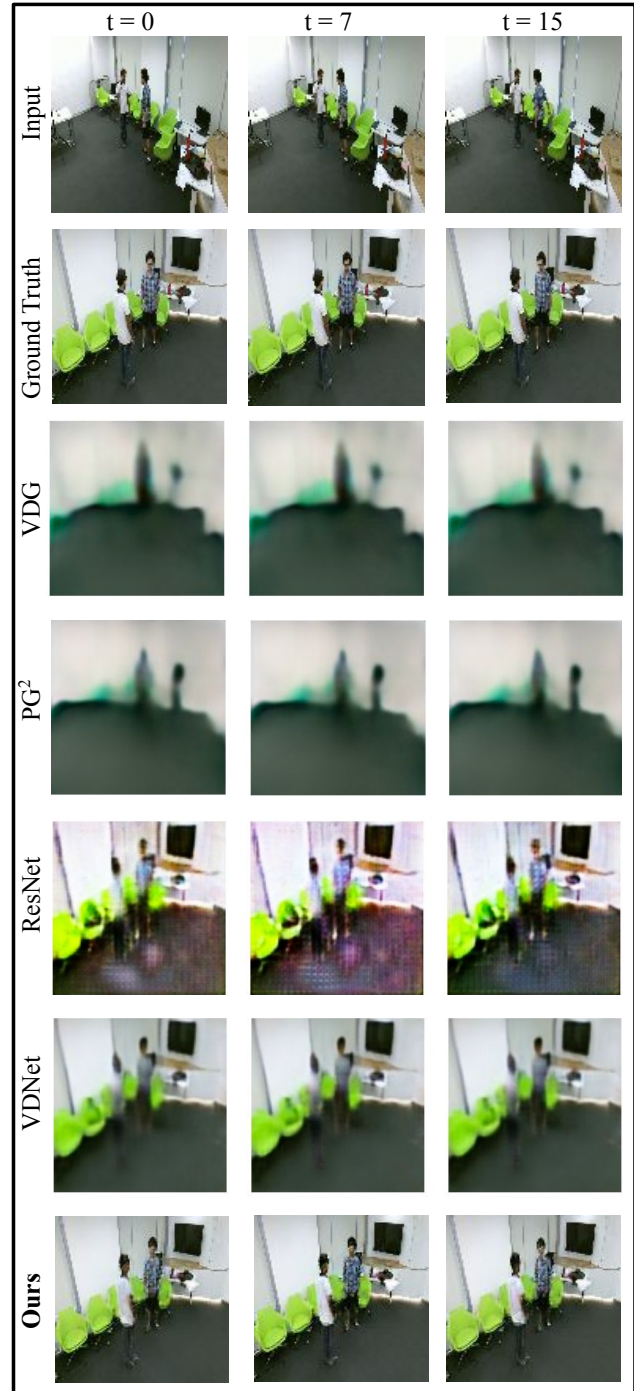


Fig. 12. Qualitative results on NTU-RGB+D Dataset [11] showing comparison with VDG [23], PG^2 [24], ResNet [25] and viewLSTM [9]. We show two samples and the resolution is 112×112 with single-view input setup.

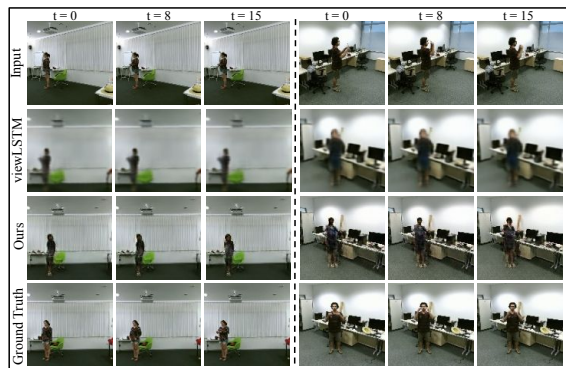


Fig. 13. Qualitative results on NTU-RGB+D Dataset[11] showing comparison with viewLSTM [9]. We show two samples and the resolution is 112×112 with single-view input setup.

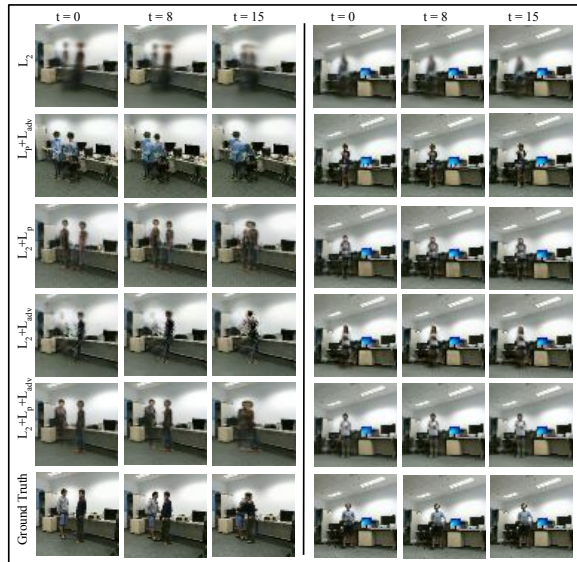


Fig. 14. Qualitative Results for loss ablations on NTU Dataset; We show frames obtained by employing different losses. We obtained the the best visual results employing all three losses ($L_2 + L_p + L_{adv}$); here L_2 : Reconstruction Loss, L_p : Perceptual Loss, L_{adv} : Adversarial Loss.